J. Fluid Mech. (2003), *vol.* 491, *pp.* 161–181.
DOI: 10.1017/S0022112003005317 Printed in the United Kingdom

Shock waves, dead zones and particle-free regions in rapid granular free-surface flows

By J. M. N. T. GRAY[1], Y.-C. TAI[2] AND S. NOELLE[3]

[1]Department of Mathematics, University of Manchester, Manchester M13 9PL, UK

[2]Institut für Mechanik, Technische Universität Darmstadt, 64289 Darmstadt, Germany

[3]Institut für Geometrie und Praktische Mathematik, Rheinisch-Westfälische Technische Hochschule Aachen, 52056 Aachen, Germany

(Received 13 September 2002 and in revised form 28 February 2003)

Shock waves, dead zones and particle-free regions form when a thin surface avalanche of granular material flows around an obstacle or over a change in the bed topography. Understanding and modelling these flows is of considerable practical interest for industrial processes, as well as for the design of defences to protect buildings, structures and people from snow avalanches, debris flows and rockfalls. These flow phenomena also yield useful constitutive information that can be used to improve existing avalanche models. In this paper a simple hydraulic theory, first suggested in the Russian literature, is generalized to model quasi-two-dimensional flows around obstacles. Exact and numerical solutions are then compared with laboratory experiments. These indicate that the theory is adequate to quantitatively describe the formation of normal shocks, oblique shocks, dead zones and granular vacua. Such features are generated by the flow around a pyramidal obstacle, which is typical of some of the defensive structures in use today.

1. Introduction

Rapid granular free-surface flows, or granular avalanches, are among the most important particle transport mechanisms in industrial processes and our natural environment. These high-density cohesionless flows down relatively flat frictional surfaces, are invariant over a surprisingly broad range of scales; starting at a few centimetres, such as pouring cornflakes into a bowl at breakfast, and going right up to geophysical scale snow-slab avalanches of up to a million cubic metres in size. In industry they often occur as part of complicated granular phase-transition flows, in which the granular material behaves as a fluid-like avalanche close to the free surface and as a solid in a large region beneath. This is typical of flows in partially filled rotating drums, which are used to mix or segregate dissimilar grains (Metcalfe *et al.* 1995; McCarthy *et al.* 1996; Gray & Hutter 1997; Hill *et al.* 1999; Shinbrot, Alexander & Muzzio 1999; Shinbrot & Muzzio 2000; Gray 2001), or whenever particles are poured out of containers or deposited to form heaps (Makse *et al.* 1997; Gray & Hutter 1998; Baxter *et al.* 1998). The magnitude of industrial applications is huge: Shinbrot & Muzzio (2000) estimate that US production alone of granular pharmaceuticals, foods and bulk chemicals amounts to a trillion kilograms per year, and most of these materials will be mixed, segregated, poured or deposited in piles at some stage of the manufacturing process.

Over the past decade significant progress has been made in the mathematical description of granular avalanches. Savage & Hutter (1989) derived a theory for the

two-dimensional plane motion of an incompressible Mohr–Coulomb material sliding down a rigid impenetrable surface, at which the body experiences dry Coulomb friction. The shallowness of the flow was exploited to integrate the leading-order mass and momentum balances through the avalanche depth to obtain a one-dimensional theory along the flow direction for the avalanche thickness and the downslope velocity. This theory was used to calculate the spreading of granular avalanches in inclined channels and the computed results and similarity solutions were in very good agreement with laboratory experiments. To calculate the flow from initiation on a steep slope to run-out on a horizontal plane, Savage & Hutter (1991) introduced a simple slope-fitted curvilinear coordinate system, which allowed the inclination angle to slowly change along the downslope direction. The theory has been able to predict key qualitative features such as the division of an avalanche into two distinct parts as it flowed over a suitably shaped bump (Greve & Hutter 1993) and the formation of normal shocks (Gray & Hutter 1997), which were not anticipated when the theory was originally formulated. The versatility of the Savage–Hutter theory has also been demonstrated by its generalization to quasi-two-dimensional depth-integrated flows down plane chutes (Hutter *et al.* 1993; Greve, Koch & Hutter 1994; Koch, Greve & Hutter 1994) and over shallow three-dimensional topography (Gray, Wieland & Hutter 1999; Wieland, Gray & Hutter 1999), as well as to steady-state flow in rotating drums (Gray 2001).

At first glance the Savage–Hutter (1989) theory has a very similar mathematical structure to the shallow-water equations of hydrodynamics. However, the constitutive properties significantly complicate the model by introducing a highly nonlinear *earth-pressure* coefficient into the theory, which pre-multiplies the pressure in the downslope momentum balance. The idea behind this term stems from a classical problem of soil loads on retaining walls in civil engineering. Savage & Hutter (1989) used the Mohr–Coulomb and basal sliding laws to show that the earth pressure is a piecewise constant function of the downslope velocity divergence. Two stress states are possible, but the Mohr–Coulomb law does not provide enough information to say which state is associated with a particular deformation. Following the retaining wall analogy the smaller active value was associated with extensive motions and the larger passive value was associated with compressive motions, and Savage & Hutter assumed that there was a jump transition between the two states when the downslope divergence was zero.

To date, there is no compelling experimental evidence to suggest that such a sharp stress transition actually takes place and it is of interest to investigate other constitutive models. An alternative hydraulic closure has been suggested in the Russian literature (Grigorian, Eglit & Iakimov 1967; Kulikovskii & Eglit 1973; Eglit 1983), by making a direct analogy between granular avalanches and shallow-water flows. Gray *et al.* (1999) and Gray (2001) have found that this simpler model also gives very promising results on steep slopes and in industrial rotating drum flows. This paper shows that the hydraulic model is sufficient to capture key qualitative features, such as shock waves, dead (no-flow) zones and particle-free regions, which commonly occur in rapid granular flows. These features are not only interesting in their own right, but contain a great deal of constitutive information that can be used to improve existing models.

2. Governing equations

The hydraulic avalanche models (Grigorian *et al.* 1967; Kulikovskii & Eglit 1973; Eglit 1983) were postulated by direct analogy with the shallow-water equations. In

order to learn more about the constitutive properties and the assumptions implicit in these models, we now generalize them to model three-dimensional depth-averaged flows over complex topography. As we shall show, there are a number of subtle differences to the assumptions present in the Savage & Hutter (1989) theory.

A fixed Cartesian coordinate system $Oxyz$ is introduced with the x-axis inclined along the downslope direction, at an angle ζ to the horizontal, the y-axis along the cross-slope direction and the z-axis is the upward pointing normal. The velocity $\boldsymbol{u}$ has components (u, v, w) in the downslope, cross-slope and normal directions, respectively. During plastic yield granular materials exhibit dilatancy effects (Reynolds 1885), but once failure has occurred and the grains are fluidized, it is reasonable to assume that material is incompressible with constant uniform density, ρ, as a first approximation. The conservative form of the mass and momentum balances reduces to

$$\nabla \cdot \boldsymbol{u} = 0, \tag{2.1a}$$

$$\rho\{\boldsymbol{u}_t + \nabla \cdot (\boldsymbol{u} \otimes \boldsymbol{u})\} = \nabla \cdot \boldsymbol{T} + \rho \boldsymbol{g}, \tag{2.1b}$$

where $\boldsymbol{T}$ is the Cauchy stress, $\otimes$ is the dyadic product, ∇ is the gradient operator, the subscript $(\,)_t$ denotes partial differentiation with respect to time t and $\boldsymbol{g}$ is gravitational acceleration.

In the Savage & Hutter (1989) theory the Cauchy stress is assumed to satisfy a Mohr–Coulomb flow law. In the hydraulic theories an isotropic pressure field, p, must clearly be included, but it is not immediately apparent that there must also be an additional deviatoric stress, $\boldsymbol{\sigma}$, to transmit the basal traction through the avalanche depth. The Cauchy stress is therefore of the form

$$\boldsymbol{T} = -p\mathbf{1} + \boldsymbol{\sigma}. \tag{2.2}$$

where $\mathbf{1}$ is the unit tensor and $\boldsymbol{\sigma}$ has components $\sigma_{xx}, \sigma_{yy}, \sigma_{zz}, \sigma_{xy}, \sigma_{xz}, \sigma_{yz}$. Derivatives will be denoted using subscript notation with the exception of the tensor components where differentiation will be denoted by the subscripts after a comma, e.g. $\sigma_{xy,z}$ is the z-derivative of σ_{xy}.

The avalanche body is subject to kinematic boundary conditions at its free surface F^s and at its base F^b,

$$\left.\begin{aligned} F^s = z - s(x, y, t) = 0: &\qquad F^s_t + \boldsymbol{u}^s \cdot \nabla F^s = 0, \\ F^b = b(x, y, t) - z = 0: &\qquad F^b_t + \boldsymbol{u}^b \cdot \nabla F^b = 0, \end{aligned}\right\} \tag{2.3}$$

where the superscripts s and b indicate the surface and base, respectively. The free surface is traction free and the base is subject to a Coulomb sliding

$$\boldsymbol{T}^s \boldsymbol{n}^s = \boldsymbol{0}, \tag{2.4a}$$

$$\boldsymbol{T}^b \boldsymbol{n}^b = \mu(\boldsymbol{n}^b \cdot \boldsymbol{T}^b \boldsymbol{n}^b)(\boldsymbol{u}^b/|\boldsymbol{u}^b|) + \boldsymbol{n}^b(\boldsymbol{n}^b \cdot \boldsymbol{T}^b \boldsymbol{n}^b), \tag{2.4b}$$

where μ is the coefficient of friction and the surface and basal normals $\boldsymbol{n}^s$ and $\boldsymbol{n}^b$ are

$$\left.\begin{aligned} \boldsymbol{n}^s &= (1/\psi^s)(-s_x, -s_y, 1), &\qquad \psi^s &= \{1 + (s_x)^2 + (s_y)^2\}^{1/2}, \\ \boldsymbol{n}^b &= (1/\psi^b)(b_x, b_y, -1), &\qquad \psi^b &= \{1 + (b_x)^2 + (b_y)^2\}^{1/2}. \end{aligned}\right\} \tag{2.5}$$

Equation (2.4*b*) simply states that basal shear traction $\boldsymbol{T}^b \boldsymbol{n}^b - \boldsymbol{n}^b(\boldsymbol{n}^b \cdot \boldsymbol{T}^b \boldsymbol{n}^b)$ is proportional to the normal traction $(\boldsymbol{n}^b \cdot \boldsymbol{T}^b \boldsymbol{n}^b)$ and resists the motion. In the Savage–Hutter theory the coefficient of friction $\mu = \tan\delta$, where δ is the basal angle of friction. This simple law describes the friction between a solid block of granular material sliding

over a relatively flat frictional base. More complicated friction laws for rougher beds (e.g. Pouliquen 1999) can, however, be easily incorporated into the theory.

The avalanche depth, H, is typically much smaller than its length, L, so that the aspect ratio $\varepsilon = H/L$ is small. This will be exploited to derive a long-wave approximation for the flow. It is convenient to introduce non-dimensional variables, which are denoted with a hat, by the following scalings:

$$\left.\begin{aligned} &(x, y, z) = L(\hat{x}, \hat{y}, \varepsilon\hat{z}), && (p) = \rho g H(\hat{p}), \\ &(u, v, w) = (gL)^{1/2}(\hat{u}, \hat{v}, \varepsilon\hat{w}), && (\sigma_{xy}, \sigma_{xz}, \sigma_{yz}) = \rho g H(\mu\hat{\sigma}_{xy}, \mu\hat{\sigma}_{xz}, \mu\hat{\sigma}_{yz}), \\ &(t) = (L/g)^{1/2}(\hat{t}), && (\sigma_{xx}, \sigma_{yy}, \sigma_{zz}) = \rho g H(\mu\hat{\sigma}_{xx}, \mu\hat{\sigma}_{yy}, \varepsilon\hat{\sigma}_{zz}). \end{aligned}\right\} \tag{2.6}$$

The scalings for the length, velocity and time are the same as those used by Savage & Hutter (1989), but those for the stress field are subtly different. The magnitude of the pressure, $\rho g H$, is set by a hydrostatic balance at the base of the avalanche; the Coulomb dry friction law (2.4b) then implies that the shear stresses are of magnitude $\mu\rho g H$. Crucially the deviatoric stress components are all assumed to be of magnitude $\mu\rho g H$, with the exception of σ_{zz}, which must be of order $\varepsilon\rho g H$ for the hydrostatic balance to hold. Typically the friction coefficient is fairly small. Savage & Hutter exploited this by assuming that $\mu = O(\varepsilon^{\gamma})$, where $0 < \gamma < 1$, which will also be assumed here.

Applying the scalings (2.6), the mass balance and momentum balance components in the downslope cross-slope and normal directions (2.1) are

$$u_x + v_y + w_z = 0, \tag{2.7a}$$

$$u_t + (u^2)_x + (uv)_y + (uw)_z = \sin\zeta + \varepsilon\mu[\sigma_{xx,x} + \sigma_{xy,y}] + \mu\sigma_{xz,z} - \varepsilon p_x, \tag{2.7b}$$

$$v_t + (uv)_x + (v^2)_y + (vw)_z = +\varepsilon\mu[\sigma_{xy,x} + \sigma_{yy,y}] + \mu\sigma_{yz,z} - \varepsilon p_y, \tag{2.7c}$$

$$\varepsilon\{w_t + (uw)_x + (vw)_y + (w^2)_z\} = -\cos\zeta + \varepsilon\mu[\sigma_{xz,x} + \sigma_{yz,y}] + \varepsilon\sigma_{zz,z} - p_z, \tag{2.7d}$$

where the hats on the non-dimensional variables are now dropped. The surface and basal kinematic conditions (2.3) become

$$s_t + u^s s_x + v^s s_y - w^s = 0, \tag{2.8a}$$

$$b_t + u^b b_x + v^b b_y - w^b = 0. \tag{2.8b}$$

At the surface the traction-free condition (2.4a) is

$$-\varepsilon\mu\left[\sigma^s_{xx}s_x + \sigma^s_{xy}s_y\right] + \mu\sigma^s_{xz} + \varepsilon p^s s_x = 0, \tag{2.9a}$$

$$-\varepsilon\mu\left[\sigma^s_{xy}s_x + \sigma^s_{yy}s_y\right] + \mu\sigma^s_{yz} + \varepsilon p^s s_y = 0, \tag{2.9b}$$

$$-\varepsilon\mu\left[\sigma^s_{xz}s_x + \sigma^s_{yz}s_y\right] + \varepsilon\sigma^s_{zz} - p^s = 0, \tag{2.9c}$$

and at the base the Coulomb friction law (2.4b) implies

$$\varepsilon\mu\left[\sigma^b_{xx}b_x + \sigma^b_{xy}b_y\right] - \mu\sigma^b_{xz} - \varepsilon p^b b_x = (\boldsymbol{n}^b \cdot \boldsymbol{T}^b \boldsymbol{n}^b)[\mu\psi_b(u^b/|\boldsymbol{u}^b|) + \varepsilon b_x], \tag{2.10a}$$

$$\varepsilon\mu\left[\sigma^b_{xy}b_x + \sigma^b_{yy}b_y\right] - \mu\sigma^b_{yz} - \varepsilon p^b b_y = (\boldsymbol{n}^b \cdot \boldsymbol{T}^b \boldsymbol{n}^b)[\mu\psi_b(v^b/|\boldsymbol{u}^b|) + \varepsilon b_y], \tag{2.10b}$$

$$\varepsilon\mu\left[\sigma^b_{xz}b_x + \sigma^b_{yz}b_y\right] - \varepsilon\sigma^b_{zz} + p^b = (\boldsymbol{n}^b \cdot \boldsymbol{T}^b \boldsymbol{n}^b)[\mu\psi_b(\varepsilon w^b/|\boldsymbol{u}^b|) - 1]. \tag{2.10c}$$

Anticipating a depth-integrated theory, the avalanche thickness h and depth-averaged value of a given function are defined as

$$h(x, y, t) = s - b, \qquad \overline{(\,)} = \frac{1}{h}\int_b^s (\,)\,\mathrm{d}z. \tag{2.11}$$

Integrating the first three conservation laws in (2.7) through the avalanche depth, using Leibnitz's rule (e.g. Abramowitz & Stegun 1970) and substituting the kinematic (2.8) and traction conditions at the surface (2.9) and base (2.10) of the avalanche, yields

$$h_t + (h\overline{u})_x + (h\overline{v})_y = 0, \tag{2.12a}$$

$$(h\overline{u})_t + (h\overline{u^2})_x + (h\overline{uv})_y - \varepsilon\mu(h\overline{\sigma_{xx}})_x - \varepsilon\mu(h\overline{\sigma_{xy}})_y + \varepsilon(h\overline{p})_x = hS^x, \tag{2.12b}$$

$$(h\overline{v})_t + (h\overline{uv})_x + (h\overline{v^2})_y - \varepsilon\mu(h\overline{\sigma_{xy}})_x - \varepsilon\mu(h\overline{\sigma_{yy}})_y + \varepsilon(h\overline{p})_y = hS^y, \tag{2.12c}$$

where the source terms on the righthand-side are

$$\left.\begin{aligned} S^x &= \sin\zeta + h^{-1}(\boldsymbol{n}^b \cdot \boldsymbol{T}^b \boldsymbol{n}^b)[\mu\psi^b(u^b/|\boldsymbol{u}^b|) + \varepsilon b_x], \\ S^y &= h^{-1}(\boldsymbol{n}^b \cdot \boldsymbol{T}^b \boldsymbol{n}^b)[\mu\psi^b(v^b/|\boldsymbol{u}^b|) + \varepsilon b_y]. \end{aligned}\right\} \tag{2.13}$$

The reduction of the equations rests on the following approximations. In the depth-integrated down- and cross-slope momentum balances (2.12*b*, *c*), terms of order ε must be retained to incorporate the longitudinal pressure gradients and ensure a non-trivial theory. Terms of order $\varepsilon\mu$ are sufficiently small, however, that they can be neglected, which eliminates gradients of the depth-integrated deviatoric stress. Integrating the normal momentum balance component (2.7*d*) with respect to z and applying the free-surface condition that $p^s = 0 + O(\varepsilon)$, implies that the leading-order pressure is hydrostatic:

$$p = (s - z)\cos\zeta + O(\varepsilon). \tag{2.14}$$

Equation (2.10*c*) therefore implies that the normal traction $\boldsymbol{n}^b \cdot \boldsymbol{T}^b \boldsymbol{n}^b = -h\cos\zeta + O(\varepsilon)$, which allows the source terms (2.13) to be approximated to order $\varepsilon\mu$. It also follows that to leading order the depth-averaged pressure

$$\overline{p} = \tfrac{1}{2}h\cos\zeta + O(\varepsilon), \tag{2.15}$$

which determines the depth-averaged longitudinal pressure gradients in (2.12). Finally, following Savage & Hutter (1989) the velocity components are assumed to be uniform through the avalanche depth

$$\left.\begin{aligned} &\overline{u} = u^b + O(\varepsilon\mu), \quad \overline{v} = v^b + O(\varepsilon\mu), \\ &\overline{u^2} = (u^b)^2 + O(\varepsilon\mu), \quad \overline{uv} = u^b\, v^b + O(\varepsilon\mu), \quad \overline{v^2} = (v^b)^2 + O(\varepsilon\mu), \end{aligned}\right\} \tag{2.16}$$

which is motivated by numerous laboratory experiments (Savage & Hutter 1989; Keller, Ito & Nishimura 1998) and field measurements (Dent *et al.* 1998). A weakness of both the Eglit (1983) and Savage–Hutter (1989) theories is that (2.16) is a model assumption rather than a rational approximation derived from the constitutive law for the deviatoric stress.

The final system of conservation laws is

$$h_t + (hu)_x + (hv)_y = 0, \tag{2.17a}$$

$$(hu)_t + (hu^2)_x + (huv)_y + \left(\tfrac{1}{2}\varepsilon h^2\cos\zeta\right)_x = hS^x, \tag{2.17b}$$

$$(hv)_t + (huv)_x + (hv^2)_y + \left(\tfrac{1}{2}\varepsilon h^2\cos\zeta\right)_y = hS^y, \tag{2.17c}$$

where the superscript b is now dropped and the source terms are

$$\left.\begin{aligned} S^x &= \sin\zeta - \mu(u/|\boldsymbol{u}|)\cos\zeta - \varepsilon b_x\cos\zeta, \\ S^y &= -\mu(v/|\boldsymbol{u}|)\cos\zeta - \varepsilon b_y\cos\zeta, \end{aligned}\right\} \tag{2.18}$$

to order $\varepsilon\mu$. The conservative system (2.17) has exactly the same mathematical structure as the shallow-water equations of hydrodynamics (e.g. Stoker 1957) and the isentropic gas-dynamics equations (e.g. Whitham 1973) when the exponent of the polytropic gas law equals 2. The key differences are that there are quite complicated source terms on the right-hand side of the equations and the pressure terms are multiplied by the factor $\cos\zeta$ to account for the reduced-gravity component on the inclined slope. It is significant that when the internal angle of friction, ϕ, is equal to the basal angle of friction, δ, the one-dimensional Savage-Hutter theory (1989, 1991) also degenerates to the shallow-water equations. All the results for the hydraulic model, therefore also hold for the Savage–Hutter model provided there are no jump stress transitions.

The analogy with shallow-water theory and gas dynamics is, as we shall see later, a very good one, and helps many frequently observed phenomena to be understood. The theory of characteristics (Courant & Hilbert 1962) implies that (2.17) is a non-strictly hyperbolic system of equations with sound velocity $c = \sqrt{\varepsilon h \cos\zeta}$. The sound velocity is equal to zero when $h = 0$, so the avalanche boundary where the thickness equals zero therefore has the same degenerate mathematical structure as the vacuum boundary in gas dynamics. Particle-free regions are therefore termed *granular vacua*. A *granular Froude number* may be defined as the ratio of the velocity to the local wave speed of the flow:

$$Fr = \frac{|\boldsymbol{u}|}{\sqrt{\varepsilon h \cos\zeta}}, \tag{2.19}$$

which distinguishes between supercritical (shooting) flows, for $Fr > 1$, and subcritical flows where $Fr < 1$. Many granular avalanches are expected to be supercritical, because the scalings imply $Fr \sim 1/\sqrt{\varepsilon} \gg 1$. This suggests that shock waves, at which there are sudden jumps in the velocity and thickness, should be common features of these flows. In the derivation of the field equations (2.17), h and $\boldsymbol{u}$ are assumed to be continuously differentiable in position and time. These conditions are not met when a shock forms and instead a control-volume argument (e.g. Chadwick 1976) is used to derive mass and momentum jump conditions:

$$[\![h(\boldsymbol{u}\cdot\boldsymbol{n} - v_n)]\!] = 0, \tag{2.20a}$$

$$[\![h\boldsymbol{u}(\boldsymbol{u}\cdot\boldsymbol{n} - v_n)]\!] + \left[\!\left[\tfrac{1}{2}\varepsilon h^2 \cos\zeta\right]\!\right]\boldsymbol{n} = 0, \tag{2.20b}$$

which hold at a non-material singular surface propagating with speed v_n along the local normal $\boldsymbol{n}$. The jump bracket $[\![f]\!] = f^+ - f^-$ is the difference between the enclosed function on the forward and rearward sides of the singular surface and the evaluation position is denoted by the superscripts '+' and '−', respectively. The jump conditions (2.20) have exactly the same form as those of the shallow-water and isentropic gas-dynamic equivalents and are not affected by the source terms, which become vanishingly small as the control-volume shrinks onto the singular surface.

3. Granular bores on non-accelerative slopes

Savage (1979) observed stationary granular jumps and Gray & Hutter (1997) saw propagating normal shocks in chute flows and at the free surface of stratification pattern experiments in granular heaps, silos and flows in partially filled slowly rotating drums. Savage (1979) presented the first analysis of the stationary granular jump and we will show here that the propagating normal shock is mathematically equivalent

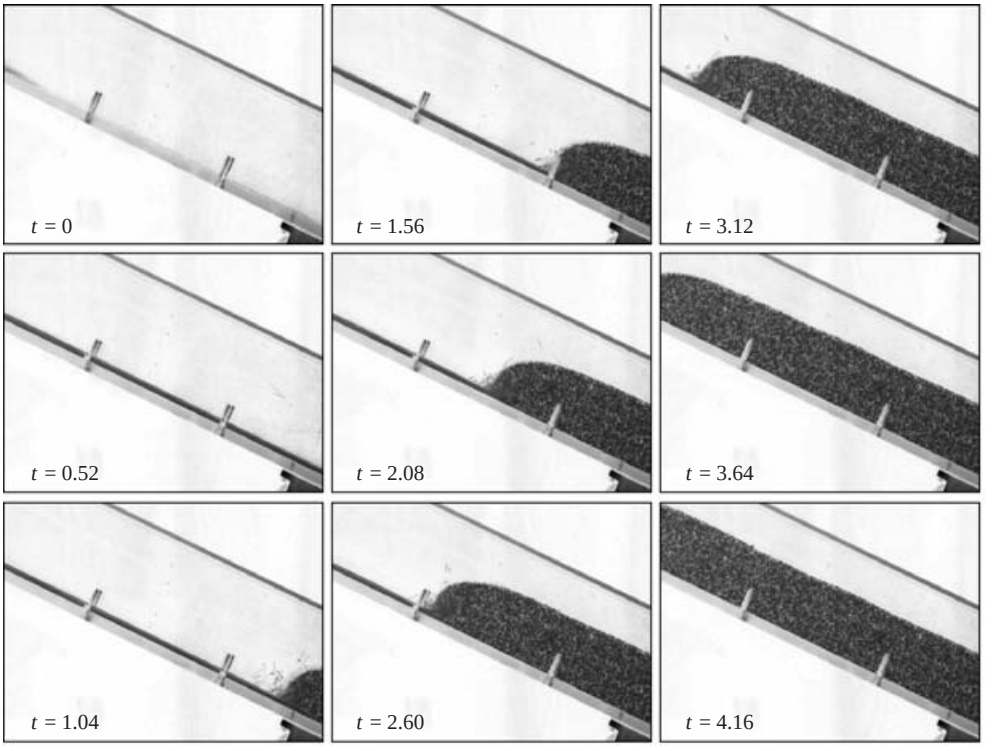

FIGURE 1. A sequence of photographs showing the upslope propagation of a granular bore, or normal shock, on a non-accelerative slope inclined at 27° to the horizontal. The images are taken every 0.52 s. The empty chute is shown top-left. A thin spatially uniform avalanche of dark (Werner's non-parielle) grains flows rapidly downslope (left-middle) and hits a wall, which is out of shot on the bottom-right side. A granular bore develops and propagates upslope at approximately constant speed, bringing the avalanche rapidly to rest and increasing its thickness by a factor of twelve as it does so. The marks normal to the chute are 17.9 cm apart. An animation of the experiment can be seen at www.ma.man.ac.uk/~ngray.

to a bore in classical hydrodynamics, which lends considerable weight to the system (2.17) and the analogy with the shallow-water equations.

Figure 1 shows a sequence of photographs of a normal shock wave in an avalanche of non-pareille† grains. The particles enter a rectangular-cross-section channel, inclined at 27° to the horizontal, and flow downslope until they hit a wall, which is out of shot at the bottom-right side. A shock wave develops and propagates upslope, bringing the particles rapidly to rest and causing the avalanche to increase dramatically in thickness. The flow has a number of important features. First, the avalanche is spatially and temporally uniform on either side of the shock, and secondly the wave propagates in the opposite direction to the flow at almost constant speed.

These observations suggest a one-dimensional solution with constant uniform states on either side of a travelling discontinuity. For the simple friction law used here, such solutions can be constructed when the slope inclination angle is equal to the basal angle of friction, $\zeta = \delta$, so that the source term $S^x = 0$ in (2.17*b*). For rough beds, there

† Non-pareille sugar grains, commonly known as '100's and 1000's' or 'Sprinkles', are roughly spherical in shape with a diameter of about 1 mm, and were supplied by Werner's Dragéefabrik, Tornesch, Germany.

is a range of angles for which steady flows develop (Pouliquen 1999; Pouliquen & Forterre 2002), but a more complex friction law must be adopted. Any slope where the gravitational acceleration is exactly balanced by the basal friction, $S^x = 0$, is non-accelerative and the field equations (2.17) admit constant uniform state solutions

$$\left.\begin{aligned} x > \xi: \quad & h(x,t) = h^+, \ u(x,t) = u^+, \\ x < \xi: \quad & h(x,t) = h^-, \ u(x,t) = u^-, \end{aligned}\right\} \tag{3.1}$$

on either side of the discontinuity at $x = \xi$. The two states may be coupled together by the mass and momentum jump conditions (2.20), which reduce in one dimension to

$$[\![h(u - v_n)]\!] = 0, \tag{3.2a}$$

$$[\![hu(u - v_n)]\!] + [\![\tfrac{1}{2}\varepsilon h^2 \cos\zeta]\!] = 0. \tag{3.2b}$$

Assuming that after the shock the grains come to rest, $u^+ = 0$, the jump conditions imply that the shock propagates with velocity

$$v_n = -\sqrt{\varepsilon \frac{h^-}{h^+}\left(\frac{h^+ + h^-}{2}\right)\cos\zeta}\,. \tag{3.3}$$

This is equivalent to the hydrodynamic bore solution given by Stoker (1957, p. 323), with an extra $\cos\zeta$ coefficient to account for reduced gravity. In the laboratory experiments the rearward and forward flow thickness are $h^- = 0.61$ cm and $h^+ = 7.29$ cm, respectively. Using (3.3) these values predict a shock velocity $v_n = -16.99\,\mathrm{cm\,s^{-1}}$, which lies within 10% of the measured velocity of $-15.4\,\mathrm{cm\,s^{-1}}$. Given the simplicity of the model, this is a very good leading-order approximation, and we therefore term the normal shock in figure 1 a *granular bore*. During rapid motion, granular materials dilate in response to inter-particle collisions, but, as the particles cross the shock, the collisional energy is rapidly attenuated and the grains settle into a denser packing. A simple mass balance argument, with the effects of density change included, is sufficient to show that when both the thickness and density increase across the shock the jump will propagate upslope at a slower speed. A relatively small density change of about 5% is sufficient to explain the difference between observed and computed shock speeds.

In the experiments there is a smooth transition between the constant uniform states on either side of the shock. This internal structure is not captured in the current model. However, it may yield important information for future theories that have a full constitutive model for the deviatoric stress. Two distinct types of shock have been observed in the experiments. At low Froude numbers the shock is diffuse as one might expect, but at high Froude numbers the shock is so sudden that some of the incoming particles rebound creating a small recirculating zone on the front face that propagates upslope with the shock.

4. Oblique shocks

The analogy between the system (2.17) and the isentropic gas-dynamics equations suggests that oblique shocks, which are common features of aerodynamic flows, should also be observed in shallow granular flows. This is indeed the case. Figure 2(*a*) shows a photograph of a steady-state oblique shock on a nearly non-accelerative slope inclined at 33° to the horizontal. The downslope coordinate lies along the horizontal axis, so that, following the gas-dynamic convention, the flow is from left to right. The

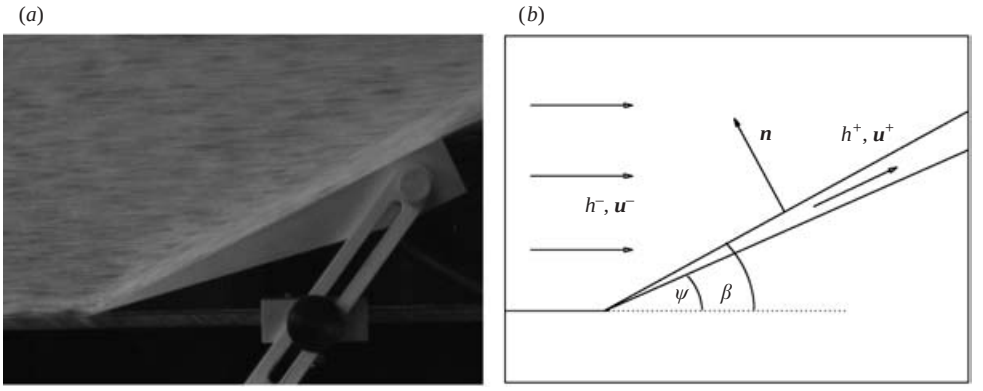

FIGURE 2. (*a*) A photograph of an oblique shock on a plane chute inclined at $\zeta = 33°$ to the horizontal. A 1/50 s exposure is used to produce streaklines aligned with the motion. (*b*) A schematic diagram of the flow. The avalanche flows downslope from left to right and is deflected by the sidewall, which is inclined inward at an angle $\psi = 25°$ to the downslope direction. A linear oblique shock develops at an angle $\beta = 29°$, creating a very thin layer of deflected material close to the wedge. The material in this layer is thicker than the incoming avalanche and flows parallel to the wedge.

shock is initiated by a sudden change in the sidewall angle, which points inward at an angle $\psi = 25°$ in the lower section of the chute. The oblique shock lies at an angle of approximately $\beta = 29°$ and the flow on the forward side of the shock is therefore confined to a very thin layer close to the deflecting sidewall, rather like hypersonic gas-dynamics flows.

In the classical oblique shock problem the field equations are satisfied by constant uniform state solutions, that are coupled together on either side of the shock by jump conditions. These simple solutions are a consequence of the fact that there are no source terms in the field equations. In general, the source terms (2.18) preclude constant state solutions to (2.17) for granular flows. However, the experiments suggest that for predominantly downslope flow on a flat-bedded nearly non-accelerative chute, the source terms may be sufficiently small that constant uniform thickness and velocity solutions, $h^+, h^-, \boldsymbol{u}^+, \boldsymbol{u}^-$, are a good local approximation to the flow. That is, we shall assume that S^x and S^y are order $\varepsilon\mu$, when $\zeta \simeq \delta$ and $u \gg v$, so that the source terms can be neglected in (2.17).

On the rearward side of the shock the velocity, $\boldsymbol{u}^- = (u^-, 0)$, whilst on the forward side the non-penetration condition requires that the flow is parallel to the wall, $\boldsymbol{u}^+ = |\boldsymbol{u}^+|(\cos\psi, \sin\psi)$. Uniformity of the flow implies that the shock lies along a straight line, which is inclined at an angle β to the downslope axis with local normal $\boldsymbol{n} = (-\sin\beta, \cos\beta)$. The mass jump condition and the tangential and normal components of the momentum jump condition (2.20) therefore imply

$$h^+|\boldsymbol{u}^+|\sin(\beta - \psi) = h^- u^- \sin\beta, \tag{4.1a}$$

$$h^+|\boldsymbol{u}^+|^2\cos(\beta - \psi)\sin(\beta - \psi) = h^- u^{-2}\cos\beta\sin\beta, \tag{4.1b}$$

$$h^+|\boldsymbol{u}^+|^2\sin^2(\beta - \psi) + \tfrac{1}{2}\varepsilon\cos\zeta(h^{+2} - h^{-2}) = h^- u^{-2}\sin^2\beta. \tag{4.1c}$$

Substituting for $h^+|\boldsymbol{u}^+|\sin(\beta - \psi)$ from (4.1*a*) equation (4.1*b*) implies that the forward and rearward velocity components parallel to the shock are unaffected by the jump in thickness, i.e. $|\boldsymbol{u}^+|\cos(\beta - \psi) = u^-\cos\beta$. Eliminating $\sin(\beta - \psi)$ between (4.1*a*) and

(4.1*c*), it follows that the shock inclination angle satisfies the relation

$$\sin\beta = \frac{1}{Fr^-}\sqrt{\frac{1}{2}\frac{h^+}{h^-}\left(\frac{h^+}{h^-}+1\right)}. \tag{4.2}$$

This takes exactly the same form as that of an oblique hydraulic jump (Chaudhry 1993, p. 173) except that the granular Froude number (2.19) accounts for reduced gravity. In the laboratory experiment, shown in figure 2, the incoming flow is 4 mm thick and has a velocity of 1.05 m/s, which implies that the granular Froude number $Fr^- = 5.79$. On the forward side of the shock the flow depth rapidly rises to 14 mm, so the thickness ratio $h^+/h^- = 3.5$ and equation (4.2) predicts that the oblique shock should be at an angle $\beta = 29.04^\circ$. This is in suprisingly good agreement with the measured angle of approximately 29°, especially considering that the incoming flow is only a few particle diameters thick and we have neglected source terms. Unlike the normal shock, the particles are still in a rapidly moving agitated state on the forward side of the shock and there are no significant density changes in this case.

5. Rapid granular flow past obstacles

The flow of granular materials past obstacles is of considerable practical interest in industrial processes, and it is especially important for the design of defences to protect buildings and structures from snow-slab avalanches, debris flows and rockfalls. By their very nature obstacles generate regions of compression and expansion in the avalanche, and a rich array of flow phenomena may be observed in laboratory experiments. These features are not only interesting in their own right, but also provide a crucial source of detailed constitutive information that can be used to test and improve existing models for rapid granular free-surface flows. It is of particular interest to see if the simple stress decomposition, into an isotropic pressure field and a less important deviatoric part in (2.2), is sufficient to qualitatively describe these types of flow, or whether there are additional effects that require the jump stress transitions in the Savage–Hutter (1989) theory.

5.1. *Flow past a forward-facing pyramid*

The flow of a granular avalanche past a tetrahedral pyramidal obstacle on a plane chute inclined at 42° to the horizontal is shown in figure 3. The shape of the obstacle is based on a defence which has been proposed for the protection of the Schneeferner Haus on the Zugspitze in Germany. The footprint of the pyramid in figure 3 is almost equilateral in shape, with sides of about 37 cm in length. The pyramid is aligned so that one of its corners points upslope and its apex is very slightly off centre, with a normal height of 16.5 cm above the chute. The granular material, which is composed of black and white plastic pellets of 2–3 mm in size, is released onto the plane from a hopper on the left-hand side and flows downslope from left to right (following the gas-dynamics convention). The avalanche front propagates rapidly downslope and remains laterally uniform prior to impinging on the pyramid. As the avalanche hits the topography the flow increases in thickness and is deflected, so that it lies parallel to the face in a very similar manner to the oblique shocks in § 4. A long-time exposure has been used to reveal the particle paths and hence the shock-like structures, which can clearly be identified in a very thin layer close to the topography in the middle-left photo of figure 3.

Outside the oblique shock region the avalanche continues to flow downslope and is unaffected by the presence of the obstacle, which is typical of supercritical hyperbolic

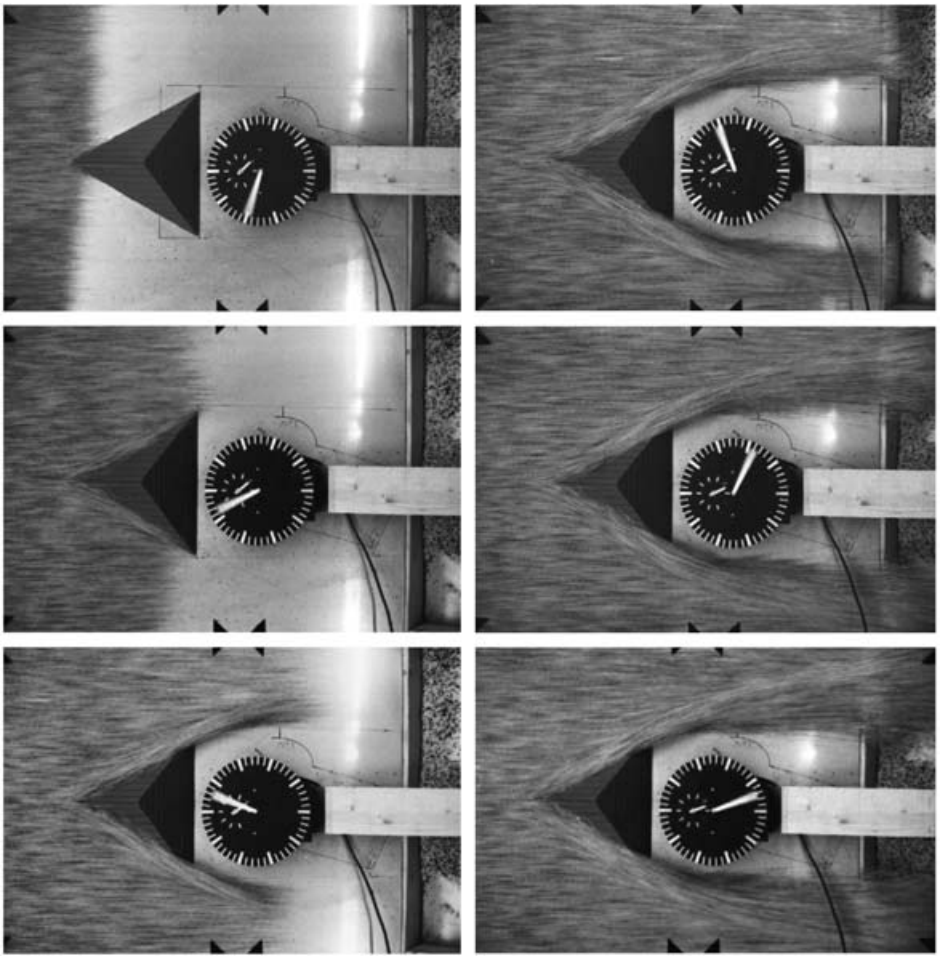

FIGURE 3. A series of photographs showing the development of a supercritical granular free-surface flow around an upslope-facing pyramid that lies on a plane inclined at 42° to the horizontal. The clock hand performs one revolution per second and the images are approximately 0.128 s apart. The flow is from left to right and a shutter speed of 1/30th of a second makes the particle paths visible. An oblique shock develops on each side of the pyramid and on the leeside two expansion waves are formed and a grain-free region opens up. A fully developed steady-state regime is reached in the bottom-right image.

flows. The avalanche front therefore remains laterally uniform a sufficiently large distance away. An interesting feature of the flow is that the position of the deflected front is slightly further downslope that the undeflected part. This has also been observed on the geophysical scale. Jóhannesson (2001) surveyed an avalanche which had been deflected by a dam at Flateyri in north-western Iceland. He found that the deflected stream came to rest 100 m further downslope than the undeflected part. This effect, although small, may be a critical consideration for designing avalanche defences.

As the avalanche passes the transition between the front faces and rear face of the pyramid the topography changes so rapidly that the avalanche briefly becomes airborne and the particles follow a ballistic trajectory. This effect is confined to a very

small region close to the rear corners of the pyramid. The avalanche is split into two separate streams and the front rapidly moves out of shot in the subsequent images.

Within a second of opening the hopper a steady-state flow develops. The final distribution is shown in the bottom-right photo of figure 3. After the flow passes the obstacle the thicker deflected flow is free to expand laterally and it slowly spreads out. The pressure is not strong enough to immediately push the particles into the region on the leeside of the pyramid and a large grain-free granular vacuum forms. In the experiments the clock is placed within the grain-free region and it is therefore protected from the avalanche. This effect is of crucial importance on a civil engineering scale, where obstacles can be used to protect buildings and structures from snow-slab avalanches and debris flows. This has been known for a long time: there is a 17th century Church in Davos, Switzerland (Ammann, Buser & Vollenwyder 1997, p. 134), which has been deliberately built with a wedge-like form to protect it from avalanches.

5.2. *Computational method*

To compute the flow around a pyramidal obstacle it is necessary to use high-resolution shock-capturing numerical methods to integrate the system (2.17). The development of these methods has a long history starting with the classic papers of Godunov (1959), Van Leer (1979), Harten (1983) and Yee (1987), and there are now a wide range of textbooks on the subject (e.g. Le Veque 1990; Godlewski & Raviart 1996; Kröner 1997; Toro 1997). Here we have opted to use the recent high-resolution shock-capturing non-oscillatory central (NOC) scheme first introduced by Nessyahu & Tadmor (1990) and extended to multi-dimensions by Arminjon & Viallon (1995, 1999); Jiang & Tadmor (1998) and Lie & Noelle (2003).

Tai *et al.* (2002) have used the NOC scheme to compute the evolution of the one-dimensional parabolic-cap similarity solution of the Savage–Hutter (1989) equations, and have found that it produces accurate results even in domains where grain-free vacuum regions are present. While it is possible to explicitly track the moving vacuum boundary in one dimension (Tai *et al.* 2002) this becomes much more complicated in multi-dimensions. The two-dimensional NOC scheme of Jiang & Tadmor (1998) is therefore used to solve the conservative system (2.17) over the entire domain including any vacuum regions. This approach provides a simple accurate scheme, but the position of the vacuum boundary is not resolved explicitly.

Full details of the NOC method are given by Jiang & Tadmor (1998) and for brevity they are not repeated here. The scheme requires the system to be rewritten in terms of conservative variables, which are the avalanche thickness h and the depth-integrated down- and cross-slope momentum, $m = hu$ and $n = hv$. In vector form, equations (2.17) then transform to

$$\boldsymbol{w}_t + \boldsymbol{f}(w)_x + \boldsymbol{g}(w)_y = \boldsymbol{s}, \tag{5.1}$$

where $\boldsymbol{w} = (h, m, n)^T$ is the vector of conservative variables. The downslope and cross-slope flux vectors, $\boldsymbol{f}$ and $\boldsymbol{g}$, and the source vector, $\boldsymbol{s}$, are given by

$$\boldsymbol{f} = \begin{pmatrix} m \\ m^2/h + \varepsilon \cos\zeta h^2/2 \\ mn/h \end{pmatrix}, \quad \boldsymbol{g} = \begin{pmatrix} n \\ mn/h \\ n^2/h + \varepsilon \cos\zeta h^2/2 \end{pmatrix}, \quad \boldsymbol{s} = \begin{pmatrix} 0 \\ hS^x \\ hS^y \end{pmatrix}. \tag{5.2}$$

The source terms, S^x and S^y, defined in (2.18), are of crucial importance, as the basal topography gradient terms determine the dynamic effect of the obstacle on the flow.

To evaluate the gradients, the normal height, $z = b(x, y)$, of the topography above the inclined plane must be prescribed. In the case of the pyramidal obstacle the normal height

$$b = \begin{cases} b_c \dfrac{(x-x_a)}{(x_c-x_a)} - \dfrac{(x_b-x_a)}{(x_c-x_a)} \dfrac{y}{y_b}, & y > 0, \quad y < y_b \dfrac{(x-x_a)}{(x_b-x_a)}, \quad y > y_b \dfrac{(x-x_c)}{(x_b-x_c)}, \\ b_c \dfrac{(x-x_a)}{(x_c-x_a)} + \dfrac{(x_b-x_a)}{(x_c-x_a)} \dfrac{y}{y_b}, & y < 0, \quad y > y_b \dfrac{(x_a-x)}{(x_b-x_a)}, \quad y < y_b \dfrac{(x_c-x)}{(x_b-x_c)}, \\ b_c \dfrac{(x-x_b)}{(x_c-x_b)}, & x < x_b, \quad y < y_b \dfrac{(x-x_c)}{(x_b-x_c)}, \quad y > y_b \dfrac{(x_c-x)}{(x_b-x_c)}, \end{cases} \tag{5.3}$$

where $(x_a, 0, 0)$ is the foremost point of the pyramid, $(x_c, 0, b_c)$ is the central point, and $(x_b, \pm y_b, 0)$ are the coordinates of the remaining two vertices. An equal horizontal and normal length scaling of 10 cm is used to convert the geometry of the experiment into non-dimensional units. The pyramid is therefore given by $x_a = 2$, $x_c = 3.95$, $x_b = 5.3$, $y_b = 1.85$ and $b_c = 1.65$ non-dimensional units.

The source terms are essentially innocuous and can easily be incorporated directly into the NOC scheme, except when $\boldsymbol{u} = \boldsymbol{0}$. When $\boldsymbol{u} = \boldsymbol{0}$ the direction of the Coulomb frictional resistance to motion, $\boldsymbol{u}/|\boldsymbol{u}|$, is not defined in (2.18). This is a case of the basic physics in the model breaking down, and we require the direction of the force to be oriented to resist the motion that the avalanche would have if the Coulomb resistance were not present. To approximate this, we assume that $\boldsymbol{u}/|\boldsymbol{u}| = \boldsymbol{0}$ when $\boldsymbol{u} = \boldsymbol{0}$ in the predictor-step of the NOC scheme to compute an intermediate value $\boldsymbol{u}^*$. In the full step $\boldsymbol{u}^*$ is then used to determine the direction of the frictional resistance.

The computational domain is rectangular in shape and extends over the range $0 \leqslant x \leqslant 12$ and $-5 \leqslant y \leqslant 5$. There are 200 grid nodes in each direction. A uniform inflow thickness and velocity is prescribed along $x = 0$, whilst outflow conditions are prescribed along all the other boundaries. For all the simulations presented here, the initial thickness is based on the first experimental image, whilst the velocity is assumed to be equal to the inflow velocity. In grain-free regions the avalanche thickness is assumed to be zero, $h(x, y, 0) = 0$, and hence the depth-integrated momentum $m(x, y, 0) = 0$ and $n(x, y, 0) = 0$.

5.3. *Computed flow past a forward-facing pyramid*

The evolution of the thickness distribution as the avalanche flows past the forward-facing pyramid is shown in figure 4, at a sequence of equal time steps approximately corresponding to those in the experiment. The experimental inflow conditions were reproduced by prescribing an inflow thickness of 0.1 units and velocity of 1.6 units, which implies that the inflow Froude number is 5.86. The chute was inclined at $\zeta = 42^\circ$ to the horizontal and the basal angle of friction $\delta = 32^\circ$. Although the vacuum boundary is not explicitly resolved, some idea of its position can be obtained by shading the region in which the avalanche thickness is above the minimum grain size of 2 mm, which corresponds to 0.02 non-dimensional units. As in the experiments the avalanche accelerates downslope and the flow remains purely one-dimensional, so that the front is laterally uniform prior to hitting the obstacle. At the pyramid the flow is divided into two streams and deflected to form oblique shock-like structures at which the thickness increases. As the avalanche flows past the back of the obstacle the flow expands and the thickness decreases again. The simulation shows that the position of the deflected front is slightly further downslope than the undeflected front

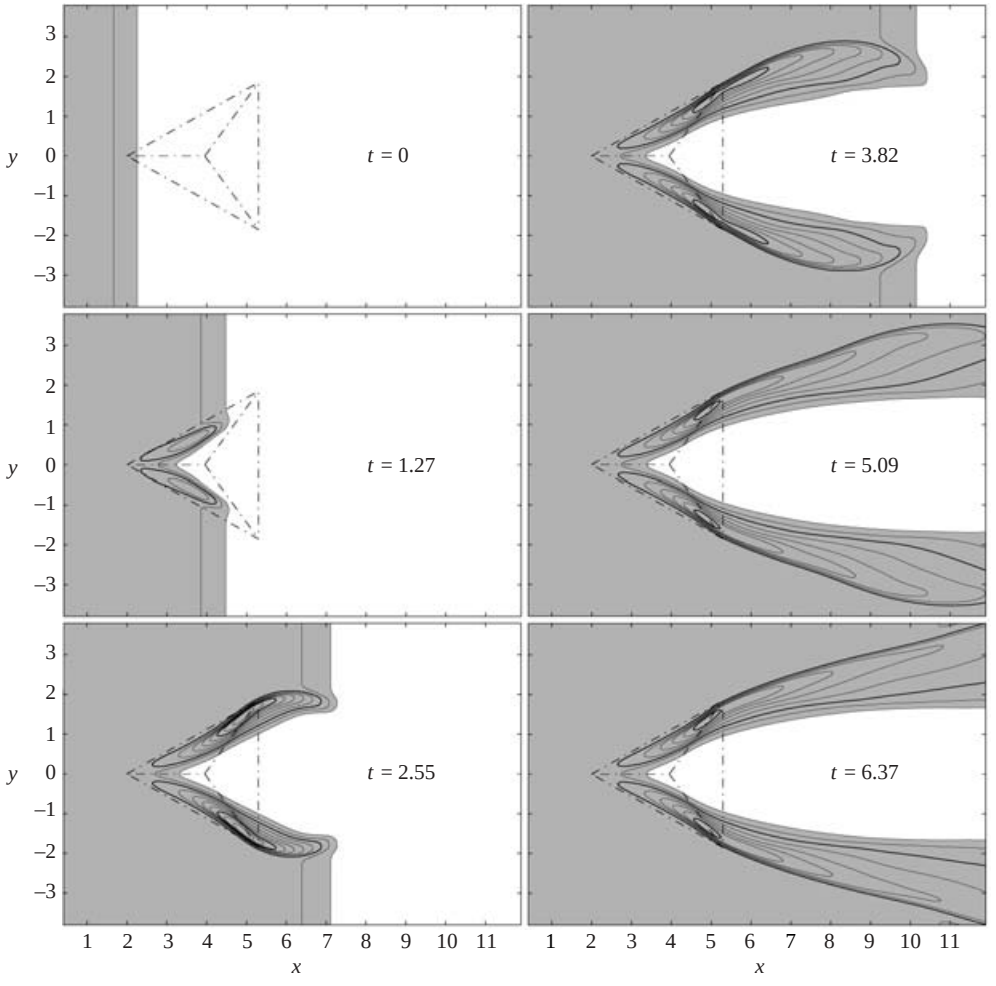

FIGURE 4. The evolution of the avalanche thickness distribution is illustrated for the upslope-facing pyramid at a sequence of time steps. The chute is inclined at 42° to the horizontal and the dot-dashed line indicates the position of the pyramid. At the inflow, at $x = 0$, the avalanche is 0.1 units thick and flowing at a velocity of 1.6 units, implying $Fr = 5.86$. The thickness contours increment in 0.04 unit intervals starting from 0.02 units, and thicker lines are used for the 0.1, 0.3, 0.5, 0.7 unit contours. For comparison with the experiment the shaded region shows the area in which the avalanche thickness is greater than the minimum particle size of 2 mm or 0.02 non-dimensional units. The time steps are chosen to be 1.2734 units apart so that the images are approximately the same interval apart as in the experiment. One non-dimensional length unit corresponds to 10 cm in the experiment.

at $t = 2.55$ units, which is in agreement with experiment and observations at the geophysical scale (Jóhannesson 2001). The primary reason for this is that the increase in thickness after the shock provides a greater pressure to push the front downslope. In the experiments the avalanche briefly becomes airborne as it flows over the rear side of the pyramid. This is not modelled in this simulation as it is implicitly assumed that the avalanche always experiences a basal Coulomb drag from being in contact with the slope. Although this is neglected it does not appear to be a significant effect in this situation.

At $t = 6.37$ units the flow has attained a steady state. The system of equations (2.17) is sufficient to capture all the qualitative features of the flow, such as the formation of the oblique shocks, expansion waves and the granular vacuum on the leeside of the pyramid. The model is also in very good quantitative agreement with experiment, both in the position of these features and the time scale for their formation. This suggests that the Savage–Hutter (1989) model could be simplified to remove the jump stress transitions between regions of convergence and divergence, as these are expected to cause additional shocks, which are not observed in experiment.

5.4. *Flow past a rearward-facing pyramid*

Many avalanche defence structures have a blunt face facing upslope, rather than a sharp one as in the forward-facing pyramid. The flow around such obstacles is more complex and new physical phenomena are introduced. To investigate this in greater detail we have taken the tetrahedral pyramid and rotated it by 180° as shown in figure 5. In non-dimensional coordinates the apex of the pyramid lies at (5.05, 0) and has a height of 1.65 units. The other vertices lie on the inclined plane at (3.7, $\pm$1.85) and (7, 0). A series of photographs of the experiment are shown in figure 5 and the corresponding computations of the avalanche thickness are shown in figure 6. The chute is inclined at $\zeta = 34°$ to the horizontal and at the inflow the avalanche is assumed to be 0.1 units thick and flows at a velocity of 1.1 units, until $t = 10.5$ units when the hopper empties and $h(0, y, t)$ is set to zero.

During the initial part of the flow, $t < 10.5$ units, the avalanche flows around the pyramid and develops into a steady state. When the flow first impinges on the front face of the pyramid the topography gradients are sufficient to bring the material to rest and form a thick stationary deposit, or *dead zone*. This is a new feature of the flow, which does not develop in gas-dynamic or shallow-water flows. In such dead zones the Coulomb basal friction balances the basal topography gradients and the internal pressure to create a stationary deposit. The dead zone grows in size until it saturates, creating a detached shock upslope of the obstacle which deflects the flow into two streams. The width of these streams is greater than in the case of the forward-facing pyramid and a considerable amount of material cascades over the edges of the front face. The simulations and experiment are nevertheless in good qualitative and quantitative agreement with one another, indicating that the simplified model (2.17) is sufficient to capture the formation of the dead zone. On the leeside of the pyramid a granular vacuum forms; however, it is much narrower and affords much less protection than the forward-facing pyramid.

When the inflow is shut off a second vacuum boundary propagates down the chute as shown at $t = 11.46$ units in figure 6. The front is laterally uniform except where the flow is deflected by the detached shock in front of the dead zone. As the front propagates past the obstacle the pressure applied to the front face of the dead zone ceases and it expands slightly upslope. By $t = 19.55$ units the cascading flow over the edges is starting to be pinched off as the vacuum boundary on the upslope and leeside of the pyramid approach each other. At subsequent times the experimental flow is reduced to individual particles trickling over the edges of the front face. While the hypothesis of an incompressible continuum breaks down, equations (2.17) still predict that material is transported over the edges. Although the dynamics of the trickling flow are not modelled well, useful predictions can still be made about the permanent deposit that is left on the blunt face of the pyramid, as shown in figure 7. The overall shape and size of the stationary deposit at $t = 45$ units is in good agreement with experiment. This is a novel feature of the flow which does not occur in gas-dynamics or shallow-water theory.

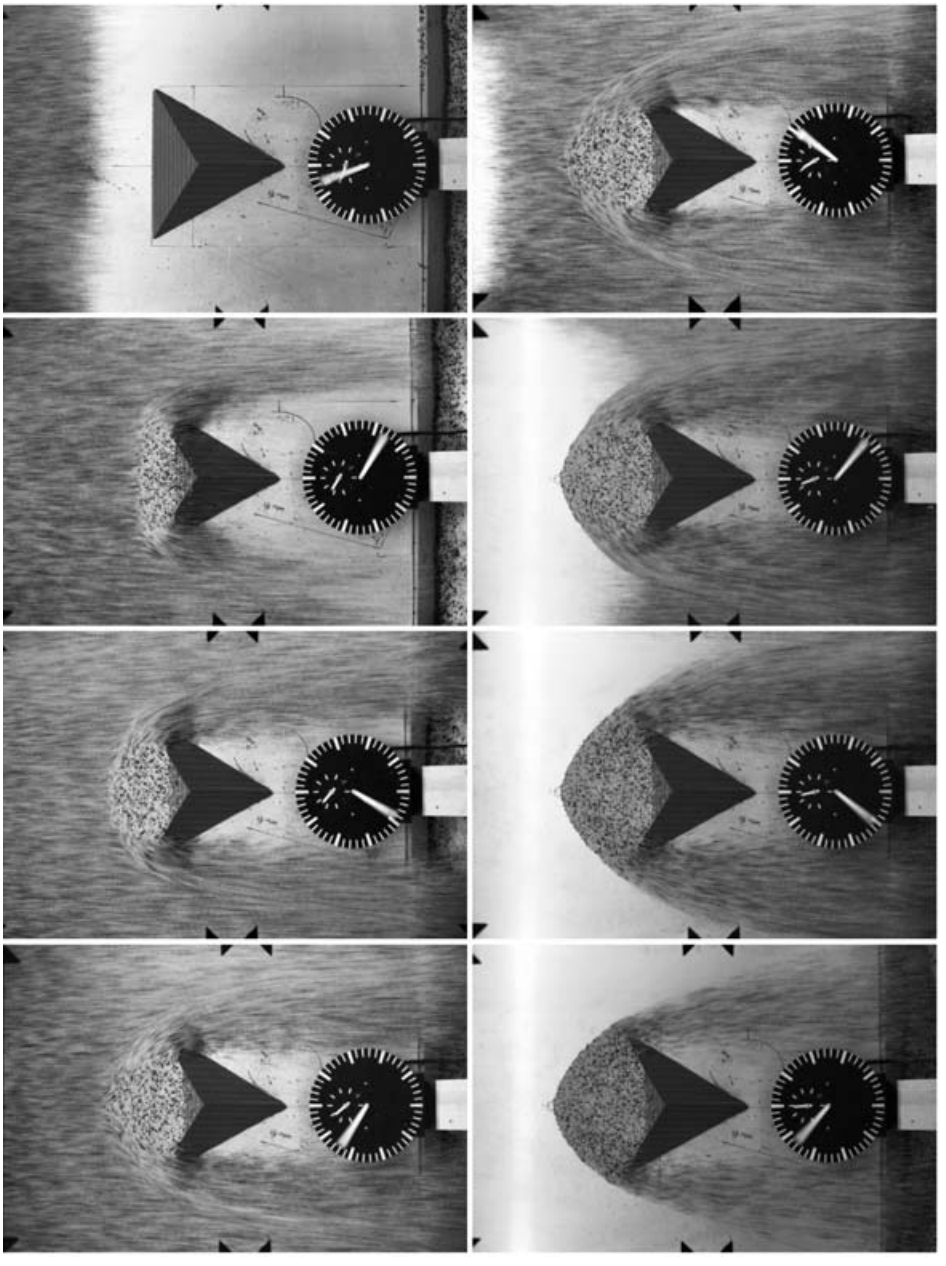

FIGURE 5. A series of photographs showing the development of a supercritical granular free-surface flow around a downslope-facing pyramid that lies on a plane inclined at 34° to the horizontal. The clock hand performs one revolution per second. The flow is from left to right and a shutter speed of 1/30th of a second makes the particle paths visible. A normal shock develops on the blunt face and propagates slowly upslope bringing the material behind it to rest. This creates a stationary dead zone in front of the pyramid that diverts the flow, whilst on the leeside a grain-free region opens up. A fully developed steady-state regime is reached in the bottom-left image. A striking feature is that, when the inflow ceases, the material in the dead zone remains on the front face of the pyramid.

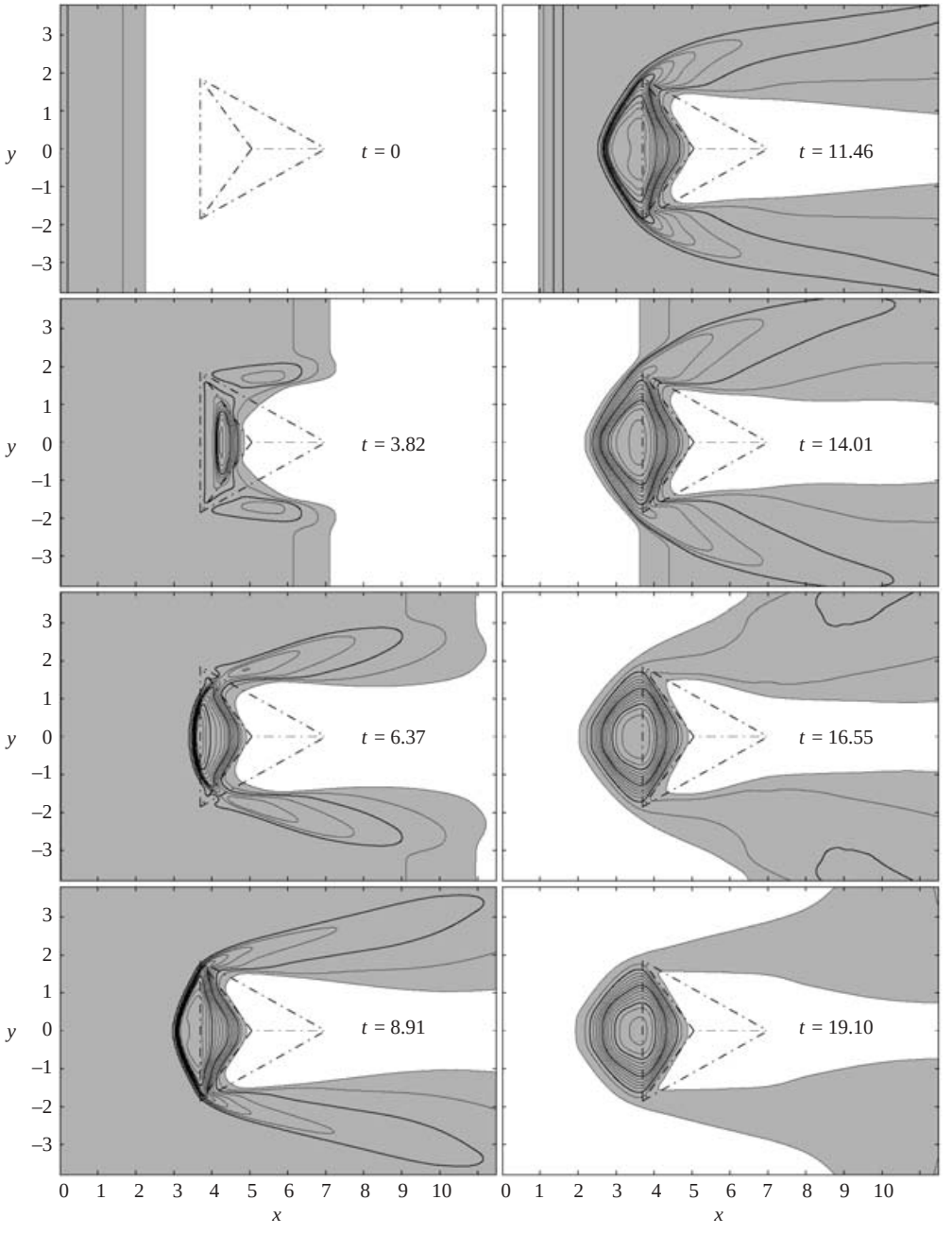

FIGURE 6. The evolution of the avalanche thickness distribution is illustrated for the downslope-facing pyramid at a sequence of time steps. The chute is inclined at 34° to the horizontal and the dot-dashed line indicates the position of the pyramid. At the inflow, at $x = 0$, the avalanche is 0.1 units thick and flowing at a velocity of 1.1 units, implying that $Fr = 3.82$. The thickness contours increment in 0.04 unit intervals starting from 0.02 units, and thicker lines are used for the 0.1, 0.3, 0.5, 0.7 unit contours. For comparison with the experiment the shaded region shows the area in which the avalanche thickness is greater than the minimum particle size of 2 mm or 0.02 non-dimensional units. The images are approximately the same interval apart as in the experiment.

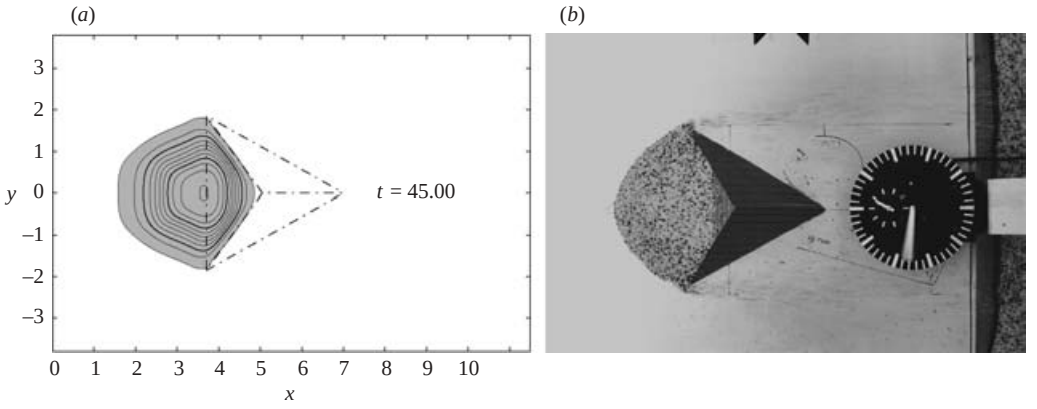

FIGURE 7. (*a*) The final computed thickness distribution of the granular material remaining in the dead zone, at $t = 45$ time units is illustrated using the same contour intervals as before. For comparison with the experiment (*b*) the shaded region shows the area in which the avalanche thickness is greater than the minimum particle size of 2 mm or 0.02 non-dimensional units.

6. Conclusions

We have generalized the hydraulic theory for granular avalanches (Grigorian *et al.* 1967; Kulikovskii & Eglit 1973; Eglit 1983) to model three-dimensional depth-averaged flows over obstacles. Although the theory is relatively simple, we have shown, by comparing exact and numerical solutions with experiments, that it contains sufficient physics to be able to capture the formation of normal shocks, oblique shocks, granular vacua and dead zones, which are frequently encountered in rapid granular free-surface flows. The small-scale laboratory results show that the stress field is dominated by a hydrostatic pressure field and a deviatoric stress, which transmits the basal shear traction through the avalanche depth.

The small-scale laboratory results show that there is no evidence of sharp stress transitions, which are expected to give rise to additional shocks at the boundary between converging and diverging flow. There is also no evidence for significant changes in the limiting stress states at these small scales. Changes in the earth-pressure coefficient are more likely to occur in geophysical-scale run-out events, where the depth of the avalanche and the stresses are significantly greater. Some evidence for this is provided by Hungr (1995), who performed numerical simulations of the 620 m high run-up of the Avalanche Lake rock avalanche (Evans, Hungr & Enegren 1994) using both hydraulic and Savage–Hutter models. He was only able to model the correct run-up by letting the earth-pressure coefficient vary during the flow over a range of 0.24 to 4.2. There may, however, be other explanations for this long run-out behaviour. On a purely theoretical level, equations (2.17) have nice properties, as they eliminate concerns about rotational symmetry of the earth-pressure coefficients and an additional velocity-dependent drag can be incorporated into the theory without the earth-pressure coefficients becoming complex valued (Gray & Tai 1998).

A high-resolution shock-capturing non-oscillatory central scheme has been developed to solve the system (2.17), and it has been used to compute the flow around a forward- and rearward-facing tetrahedral pyramid. These shapes are typical of snow-slab avalanche defences, such as the one proposed for the protection of the

Schneeferner Haus on the Zugspitze. The code can easily be applied to other obstacles, and the qualitative and quantitative agreement between theory and experiment are sufficiently good to suggest that it may be used as a tool to optimize the design of real avalanche defences.

This research was supported by the Engineering and Physical Sciences Research Council grant GR/R75304/01 and by the Deutsche Forschungsgemeinschaft through SFB 298 "Deformation und Versagen bei metallischen und granularen Strukturen" and SPP 322 "Analysis und Numerik von Erhaltungssätzen". Nico Gray would like to dedicate this paper to J. K. & E. M. J. Gray.

REFERENCES

Abramowitz, M. & Stegun, I. 1970 *Handbook of Mathematical Functions,* 9th Edn, 3.3.7. Dover.

Ammann, W., Buser, O. & Vollenwyder, U. 1997 *Lawinen.* Birkhäuser.

Arminjon, P. & Viallon, M. C. 1995 Généralisation du schéma de Nessyahu–Tadmor pour une équation hyperbolique à deux dimensions d'espace. *C. R. Acad. Sci. Paris* **320**, 85–88.

Arminjon, P. & Viallon, M. C. 1999 Convergence of a finite volume extension of the Nessyahu–Tadmor scheme on unstructured grids for a two-dimensional linear hyperbolic equation. *SIAM J. Numer. Anal.* **36**, 738–771.

Baxter, J. Tüzün, U., Heyes, D., Hayati, I. & Fredlund, P. 1998 Stratification in poured granular heaps. *Nature* **391**, 136.

Chadwick, P. 1976. *Continuum Mechanics. Concise Theory and Problems.* George Allen & Unwin (republished Dover 1999).

Chaudhry, M. H. 1993 *Open-Channel Flow*. Prentice-Hall.

Courant, R. & Hilbert, D. 1962 *Methods of Mathematical Physics. Part II. Partial Differential Equations.* Interscience, John Wiley and Sons.

Dent, J. D., Burrel, K. J., Schmidt, D. S., Louge, M. Y., Adams, E. E. & Jazbutis, T. G. 1998. Density, velocity and friction measurements in a dry-snow avalanche. *Annal. Glac.* **26**, 247–252.

Eglit, M. E. 1983 Some mathematical models of snow avalanches. In *Advances in Mechanics and the Flow of Granular Materials* (ed. M. Shahinpoor), vol. 2, pp. 577–588. Clausthal-Zellerfeld and Gulf Publishing Company.

Evans, S. G., Hungr, O. & Enegren, E. G. 1994 The Avalanche Lake rock avalanche, Mackensie Mountains, Northwest Territories, Canada: description, dating and dynamics. *Can. Geotech. J.* **31**, 749–768.

Godlevski, E. & Raviart, P.-A. 1996 *Numerical Approximation of Hyperbolic Systems of Conservation laws.* Springer.

Godunov, S. 1959 A finite difference scheme for numerical computation of the discontinuous solutions of equations of fluid dynamics. *Math. Sb.* **47**, 271–306.

Greve, R. & Hutter, K. 1993 Motion of a granular avalanche in a convex and concave curved chute: experiments and theoretical predictions. *Phil. Trans. R. Soc. Lond.* A **342**, 573–600.

Greve, R., Koch, T. & Hutter, K. 1994 Unconfined flow of granular avalanches along a partly curved surface. Part I: Theory. *Proc. R. Soc. Lond.* A **445**, 399–413.

Gray, J. M. N. T. 2001 Granular flow in partially filled slowly rotating drums. *J. Fluid. Mech.* **441**, 1–29.

Gray, J. M. N. T. & Hutter K. 1997 Pattern formation in granular avalanches. *Continuum Mech. & Thermodyn.* **9**, 341–345.

Gray, J. M. N. T. & Hutter, K. 1998 Physik granularer Lawinen. *Physikalische Blätter* **54**, 37–43.

Gray, J. M. N. T. & Tai, Y. C. 1998 On the inclusion of a velocity dependent basal drag in avalanche models. *Annal. Glac.* **26**, 277–280.

Gray, J. M. N. T., Wieland, M. & Hutter K. 1999 Free surface flow of cohesionless granular avalanches over complex basal topography. *Proc. R. Soc. Lond.* A **455**, 1841–1874.

Grigorian, S. S., Eglit, M. E. & Iakimov, Iu. L. 1967 New statement and solution of the problem of the motion of snow avalanche. In *Snow, Avalanches & Glaciers. Tr. Vysokogornogo Geofizich Inst*. **12**, 104–113. (In Russian.)

Harten, A. 1983 High resolution schemes for hyperbolic conservation laws. *J. Comput. Phys.* **49**, 357–393.

Hill, K. M., Kharkar, D. V., Gilchrist, J. F., McCarthy, J. J. & Ottino, J. M. 1999 Segregation-driven organization in chaotic granular flows. *Proc. Natl Acad. Sci. USA* **96** (21), 11 689–12 210.

Hungr, O. 1995 A model for the runout analysis of rapid flow slides, debris flows and avalanches. *Can. Geotech. J.* **32**, 610–623.

Hutter, K., Koch, T., Plüss C. & Savage, S. B. 1995 The dynamics of avalanches of granular materials from initiation to run-out. *Acta Mech.* **109**, 127–165.

Hutter, K., Siegel, M., Savage, S. B. & Nohguchi, Y. 1993 Two-dimensional spreading of a granular avalanche down an inclined plane. Part I Theory. *Acta Mech.* **100**, 37–68.

Jiang, G. & Tadmor, E. 1997 Non-oscillatory central schemes for multidimensional hyperbolic conservation laws. *SIAM J. Sci. Comput.* **19**, 1892–1917.

Jóhannesson, T. 2001 Run-up of two avalanches on the deflecting dams at Flateyri, northwestern Iceland. *Annal. Glac.* **32**, 350–354.

Keller, S., Ito, Y. & Nishimura, K. 1998 Measurements of the vertical velocity distribution in ping pong ball avalanches. *Annal. Glac.* **26**, 259–264.

Koch, T., Greve, R. & Hutter, K. 1994 Unconfined flow of granular avalanches along a partly curved chute. II. Experiments and numerical computations. *Proc. R. Soc. Lond.* A **445**, 415–435.

Kröner, D. 1997 *Numerical Schemes for Conservation Laws*. Wiley-Teubner.

Kulikovskii, A. G. & Eglit, M. E. 1973 Two-dimensional problem of the motion of a snow avalanche along a slope with smoothly changing properties. *Prikl. Mat. Mekh.* **37** (5), 837–848 (in Russian: English transl. *J. Appl. Maths Mech.* **37** (5), 792–803.

Le Veque, R. J. 1990 *Numerical Methods for Conservation Laws*. Birkhäuser.

Lie, K. A. & Noelle, S. 2003 An improved quadrature rule for the flux-computation in staggered central difference schemes in multidimensions. *J. Sci. Comput.* **18**, 69–81.

McCarthy, J. J., Wolf, J. E., Shinbrot, T. & Metcalfe, G. 1996 Mixing of granular materials in slowly rotating containers. *AIChE J.* **42**, 3351–3363.

Makse, H. A., Havlin, S., King, P. R. & Stanley, H. E. 1997 Spontaneous stratification in granular mixtures. *Nature* **386**, 379–382.

Metcalfe, G, Shinbrot, T, McCarthy, J. J. & Ottino, J. M. 1995 Avalanche mixing of granular solids. *Nature* **374**, 39–41.

Nessyahu, H. & Tadmor, E. 1990 Non-oscillatory central differencing for hyperbolic conservation laws. *J. Comput. Phys.* **87**, 408–463.

Pouliquen, O. 1999 Scaling laws in granular flows down rough inclined planes. *Phys. Fluids* **11**, 542–548.

Pouliquen, O. & Forterre, Y. 2002 Friction law for dense granular flows: application to the motion of a mass down a rough inclined plane. *J. Fluid Mech.* **453**, 133–151.

Reynolds, O. 1885 On the dilatency of media composed of rigid particles in contact. *Phil. Mag.* **20**, 469–481.

Savage, S. B. 1979 Gravity flow of cohesionless granular materials in chutes and channels. *J. Fluid Mech.* **92** , 53–96.

Savage, S. B. & Hutter, K. 1989 The motion of a finite mass of granular material down a rough incline. *J. Fluid Mech.* **199**, 177–215.

Savage, S. B. & Hutter, K. 1991 The dynamics of avalanches of granular materials from initiation to run-out. Part I: Analysis. *Acta Mechanica* **86**, 201–223.

Shinbrot, T., Alexander, A. & Muzzio, F. J. 1999 Spontaneous chaotic granular mixing. *Nature* **397**, 675.

Shinbrot, T. & Muzzio, F. J. 2000 Nonequilibrium patterns in granular mixing and segregation. *Physics Today* March 2000, 25–30.

Stoker, J. J. 1957 *Water Waves*. Interscience.

Tai, Y.-C., Noelle, S., Gray, J. M. N. T. & Hutter, K. 2002 Shock capturing and front tracking methods for granular avalanches. *J. Comput. Phys.* **175**, 269–301.

Toro, E. F. 1997 *Riemann Solvers and Numerical Methods for Fluid Dynamics*. Springer.

Van Leer, B. 1979 Towards the ultimate conservative difference scheme V. *J. Comput. Phys.* **32**, 101–136.

Whitham, G. B. 1973 *Linear and Non-linear Waves.* John Wiley & Sons.

Wieland, M., Gray, J. M. N. T. & Hutter, K. 1999 Channelized free-surface flow of cohesionless granular avalanches in a chute with shallow lateral curvature. *J. Fluid Mech.* **392**, 73–100.

Yee, H. C. 1987 Construction of explicit and implicit symmetric TVD schemes and their applications. *J. Comput. Phys.* **68**, 151–179.